Nonplanar Heme Deformations and Excited State Displacements in Nickel Porphyrins Detected by Raman Spectroscopy at Soret Excitation

Qing Huang,[†] Craig J. Medforth,[‡] and Reinhard Schweitzer-Stenner*[,†]

Department of Chemistry, Drexel University, 3141 Chestnut Street, Philadelphia, Pennsylvania 19104, and Advanced Materials Laboratory, Sandia National Laboratories, 1001 University Boulevard SE, Albuquerque, New Mexico 87106

Received: June 5, 2005; In Final Form: September 17, 2005

We have correlated the Raman intensities of out-of-plane modes of nickel porphyrins with the nonplanar deformations of specific symmetries, i.e., static normal coordinate deformations (SNCDs) expressed in terms of irreducible representations of the unperturbed D_{4h} point group. The model porphyrins Ni(II) octaethyltetraphenylporphyrin (NiOETPP), Ni(II) tetra(isopropyl)porphyrin (NiT(^{i}Pr)P), Ni(II) tetra(*tert*-butyl)porphyrin (NiT(^{t}Bu)P), and Ni(II) meso-tetraphenylporphyrin (NiTPP) were chosen because they exhibit significant out-of-plane deformations of different symmetries. At B-band excitation, the Raman scattering of out-of-plane modes becomes activated mostly via the Franck−Condon mechanism. Some characteristic bands from out-of-plane modes in the spectra were identified as reliable predictors of the type and magnitude of out-of-plane deformation. The $\gamma_{10}-\gamma_{13}$ bands are indicators of ruffling (B_{1u}) deformations for porphyrins, as confirmed by data for NiTPP, NiT(^{i}Pr)P, and NiT(^{t}Bu)P, where the Raman intensity increases with the magnitude of the ruffling deformation. The $\gamma_{15}-\gamma_{17}$ bands are indicators of saddling (B_{2u}) deformations, as shown by data for NiOETPP, which is highly saddled. By comparing the relative intensities of these prominent Raman bands we estimated the vibronic coupling parameters using a self-consistent analysis, and showed that they reproduce the respective B-band absorption profiles. We also identified the deformations along the lowest wavenumber normal coordinates as the predominant reason for the Raman activity of out-of-plane modes. Our results suggest that some of the normal coordinates (γ_{10} and γ_{13}) may be used as tools to quantitatively probe the nonplanar deformations of metalloporphyrins with alkyl substituents at the *meso*-positions. Out-of-plane deformations also increase the vibronic coupling strength of some low frequency in-plane Raman modes, namely, ν_7 and ν_8. Generally, the Raman data suggest that the excited B-state is substantially more nonplanar than the ground state. The overall larger vibronic coupling of ruffled porphyrins yields substantially larger dipole strengths for the vibronic sidebands associated with the B-state transition, so that the relative absorptivity of the B_v band can be used as a convenient tool to probe the nonplanarity of the porphyrin macrocycle.

Introduction

Metalloporphyrins play an importance role in biological systems such as hemoglobin, myoglobin, cytochromes, enzymes, and photoreaction centers, where they serve as active sites which function to bind ligands, facilitate light harvesting and electron transfer, and catalyze biochemical reactions.[1] A detailed knowledge of factors determining the physical and chemical properties of the metalloporphyrin macrocycle is indispensable for a thorough understanding of these various types of reactivity. Multiple lines of evidence suggest that out-of-plane (oop) distortions of the porphyrin macrocycle are one of several factors which can influence functional properties, and oop distortions are known to modulate axial ligand affinities,[2] electron transfer rates,[3] and the oxidation potentials of various cytochromes.[4]

Thus far, the identification and quantitative determination of nonplanar deformations of metalloporphyrins has relied mostly on high-resolution X-ray structures.[5] However, these data are not always available, at least not for all spin, oxidation, and ligation states of the iron−porphyrins in heme proteins. For individual porphyrins, the structure can also be slightly different in solution and in a crystal environment.[6−8] Moreover, for heme proteins, this dependence on X-ray data does not readily permit quantitative monitoring of structural changes caused by factors such as changes in temperature, pH, or ionic strength. It is therefore desirable to identify alternative experimental means to explore these types of oop distortions, which we will refer to as static normal coordinate deformations (SNCDs). Polarized resonance Raman spectroscopy is generally an excellent tool to probe structural perturbations causing deviations from the ideal D_{4h} symmetry of the macrocycle. The correlation of depolarization ratio (DPR) of various in-plane (ip) modes with ip deformations has been well established and summarized.[9] Such DPR measurements have been applied extensively for structural perturbation studies of heme proteins, for example, in horseradish peroxidase.[10,11] In addition, the presence of oop deformations induces Raman activity of oop modes of the same symmetries, thus the analysis of Raman intensities of oop modes can be extended to the identification of oop deformations, as recently demonstrated for myoglobin cyanide[12] and horseradish peroxidase.[13]

* Corresponding author. Mailing address: Department of Chemistry, Drexel University, 3141 Chestnut Street, Philadelphia, PA 19104. E-mail: RSchweitzer-Stenner@drexel.edu.
† Drexel University.
‡ Sandia National Laboratories.

10.1021/jp052986a CCC: $30.25
Published on Web 10/29/2005

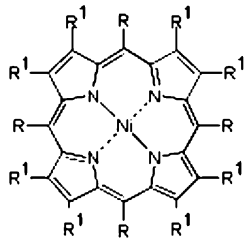

NiOEP	R = H, $R^1 = CH_2CH_3$
NiTPP	$R = C_6H_5$, R^1 = H
NiT(tBu)P	$R = C(CH_3)_3$, R^1 = H
NiT(iPr)P	$R = CH(CH_3)_2$, R^1 = H
NiOETPP	$R = C_6H_5$, $R^1 = CH_2CH_3$

Figure 1. Structure of nickel porphyrins investigated.

In the present study, we utilize polarized resonance Raman spectroscopy to explore the relationship between the Raman activity of oop modes and the oop deformations of different synthetic nickel porphyrins such as Ni(II) octaethyltetraphenylporphyrin (NiOETPP), Ni(II) tetra(isopropyl)porphyrin (NiT(^{i}Pr)P), Ni(II) tetra(*tert*-butyl)porphyrin (NiT(^{t}Bu)P), and Ni(II)tetraphenylporphyrin (NiTPP) (Figure 1). Shelnutt, Jentzen, and co-workers have developed an algorithm to describe porphyrin nonplanarity in terms of SNCDs classified in terms of the irreducible representations A_{1u}, A_{2u}, B_{1u}, B_{2u}, and E_g of the D_{4h} point group (normal coordinate structural decomposition, NSD).[14,15] For apparent physical reasons, the contribution for a distinct symmetry is dominated by the deformation along the coordinates of the respective lowest frequency mode.[14] The substantial red-shifts of B- and Q-bands in the UV−vis spectra of highly nonplanar Ni(II) porphyrins suggest that SNCDs have a substantial influence on the electronic properties of the macrocycle.[16] More recently, Haddad et al.[17] discovered that the large B-band red-shift (40 nm) observed for the highly ruffled *meso*-tetra(*tert*-butyl)porphyrin compared to *meso*-tetra(methyl)porphyrin resulted to a significant extent from deformations along the coordinates of the second ($2B_{1u}$) and third lowest ($3B_{1u}$) B_{1u}-type normal vibrations, even though these deformations require higher distortion energies and are thus an order of magnitude smaller than the observed total ruffling, which is dominated by the $1B_{1u}$ deformation.[14]

We have measured the low frequency resonance Raman spectra of the four synthetic nickel porphyrins listed above with Soret excitation (442 nm). From the assignments of distinct Raman bands to oop modes and the depolarization ratios of these bands, we obtained the symmetry type of the out-of-plane deformation. We further determined the relative intensities of all detectable Raman lines by means of an internal standard line, the 286 cm^{-1} line of the CH_2Cl_2 solvent. A self-consistent analysis of the obtained Raman intensities and the optical absorption spectrum yielded the respective vibronic coupling parameters of both ip and oop porphyrin modes. The coupling parameters of the oop modes were further analyzed to estimate minimal values for the corresponding nonplanar deformations. Thus, we were able to identify the deformations which are predominantly responsible for the Raman activity of oop modes. By using the SNCDs of the investigated porphyrins reported by Shelnutt and co-workers,[14,15] we estimated the expectation values of the vibronic coupling parameters, which provide information about excited state displacements and can be used for the structural analysis of (nickel) porphyrins.

Theoretical Background

The basic theory on which our analysis is based has been published in earlier papers.[9,18] Herein, we confine ourselves to describing only the most relevant physical parameters.

In order to account for such symmetry lowering deformations, the vibronic coupling operator $\partial\hat{H}_{el}(q,Q)/\partial q^{\tilde{\Gamma}_r'}$ of a Raman active porphyrin macrocycle vibration $Q_r^{\tilde{\Gamma}_r}$ ($\tilde{\Gamma}_r$ is now the representation in the lower symmetry group) has to be expanded into a Taylor series with respect to the normal coordinates of the induced distortions:

$$\frac{\partial\hat{H}_{el}(q,Q)}{\partial Q_r^{\tilde{\Gamma}_r'}} = \frac{\partial\hat{H}_{el0}(q,Q)}{\partial Q_r^{\Gamma_r}} + \sum_{\Gamma_i}\sum_{i}\frac{\partial^2\hat{H}_{el0}(q,Q)}{\partial Q_r^{\Gamma_r}\partial Q_i^{\Gamma_i}}\delta\bar{Q}_i^{\Gamma_i} \quad (1)$$

where $\delta\bar{Q}_i^{\Gamma_i}$ is the ith SNCD of symmetry Γ and $\hat{H}_{el0}$ is the pure electronic Hamiltonian in D_{4h} symmetry. As shown in recent analyses of isolated porphyrins and heme groups in various proteins, the set of $\delta\bar{Q}_i^{\Gamma_i}$ is dominated by deformations along the normal coordinates of the lowest frequency modes of the respective symmetry representations,[19] because the required deformation energy is proportional to the square of the respective frequencies.[14] The second term in eq 1 accounts for the resonance Raman activity of oop modes due to the presence of out-of-plane deformations. For example, B_{2u}-type modes, which are inactive in D_{4h}, can become Raman active by a deformation of the same symmetry type exerted on the macrocycle, since $\Gamma_r' = B_{2u} \otimes B_{2u} = A_{1g}$. Hence, these oop modes become Franck−Condon active, yielding additional polarized bands ($\rho = 0.125$) in the Raman spectra obtained with Soret excitation.

The vibronic coupling contribution to the Raman cross section is expressed in terms of the parameter

$$c_{lm}^{\Gamma_r} = H_{lm}^r Q_r \quad (2)$$

which contains the vibronic coupling matrix element $H_{lm}^r = \langle l|\partial\hat{H}_{el}(q,Q)/\partial Q_r^{\tilde{\Gamma}_r'}|m\rangle$ ($|l\rangle,|m\rangle = |Q_{x,y}\rangle,|B_{x,y}\rangle$) and the vibrational transition matrix element $Q_r = \langle 0|Q_r|1\rangle$ with $|0\rangle$ and $|1\rangle$ denoting vibrational states of the considered Raman active mode of the electronic ground state. It describes the changes of the excited electronic states caused by the rth vibration of the porphyrin. As above, Γ_r denotes the symmetry representation of the Raman active vibration.

The determination of the vibronic coupling parameters $c_{lm}^{\Gamma_r}$ generally requires the combined analysis of resonance excitation profiles, depolarization ratio dispersion, and absorption profiles.[31] For the present study, we adopted a somewhat simpler approach as used in the recent investigation of horseradish peroxidase C (HRP C),[13] for which we modeled the depolarization ratio dispersion of several structure sensitive ip modes by utilizing earlier obtained coupling constants of Ni(II) porphine[20] and Ni(II) octaethyltetraphenylporphyrin.[31] We focused on Raman scattering by oop modes at Soret excitation, for which the intensity arises mainly from B-state coupling.[18] This comprises Franck−Condon coupling for all modes with an A_{1g}-type Raman tensor and Jahn−Teller coupling for modes with B_{1g}- and B_{2g}-tensors. We neglected interstate Herzberg−Teller. The depolarization ratios of the Raman bands of the oop modes considered in this study are all indicative of a predominant A_{1g}-type Franck−Condon coupling, which arises from $\Gamma_r \otimes \Gamma_i = A_{1g}$, with Γ_r and Γ_i having the same symmetry, in the second term of the Taylor expansion described by eq 1. Since this term is second order with respect to the nuclear coordinates, the coupling constants can be expected to be an

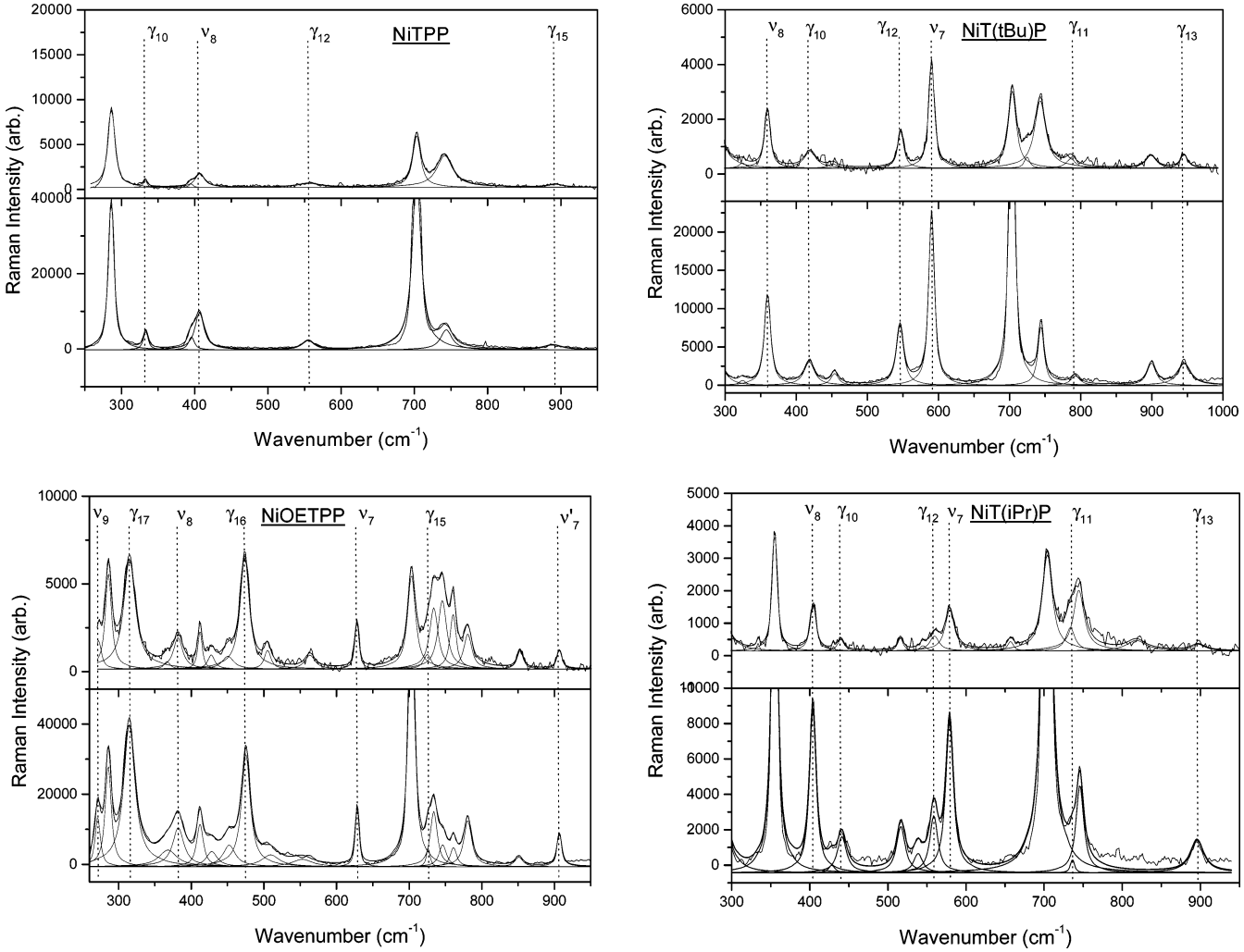

Figure 2. Low frequency polarized resonance Raman spectra of the nickel porphyrins in CH_2Cl_2. The spectra were obtained with an excitation wavelength of 442 nm, power <10 mW, and spectral resolution ca. 4 cm^{-1}. Spectra taken with a polarization perpendicular to the scattering plane are shown in the respective upper panels, those measured with parallel polarization in the lower panels.

order of magnitude smaller than those of the ip modes.[20] As mentioned above, we neglected multimode mixing, an allowed approximation if the excitation wavelength is on the low energy side of the Soret band.[31]

Materials and Methods

Sample Preparation. Ni(II) octaethylporphyrin (NiOEP) and Ni(II) tetraphenylporphyrin were purchased from Frontier Scientific, and Ni(II) octaethyltetraphenylporphyrin,[16] Ni(II) tetra(isopropyl)porphyrin,[35] and Ni(II) tetra(*tert*-butyl)porphyrin[35] were synthesized using the methods described previously. Dichloromethane (99.9%, Pharmco) was used as a solvent for measuring the Raman spectra. The porphyrin concentration in the Raman samples ranged from 0.1 to 0.5 mM. The absorption spectra were measured by diluting these samples by a factor of 100.

Spectroscopy. The equipment and the experimental conditions for our UV/vis absorption and resonance Raman measurements and the spectral analysis with MULTIFIT are described in detail in an earlier publication.[21]

Structural Deformation Analysis. We analyzed the structures of the nickel porphyrins to obtain the deformations along the normal coordinates (NSD: normal coordinate structural decomposition).[14,22−24] The structures of the porphyrins were obtained from respective crystallographic data, except for NiT(^{t}Bu)P, where the crystal structure is unavailable and the energy-minimized molecular mechanics structure was used.[17]

Results and Discussion

This section is organized into three parts. First, we present the Raman spectra of the investigated porphyrins, in which we identify the bands resulting from oop vibrations based on normal mode calculations. In the second section, we describe how the vibronic coupling parameters of all observed Raman bands were obtained by a self-consistent analysis of their intensities and B-band absorption. Finally, the coupling parameters are used to discuss excited state displacements and to quantitatively estimate the distortions which cause the observed Raman activity of the out-of-plane modes.

Resonance Raman Spectra. Figure 2 depicts the low wavenumber resonance Raman spectra of the nickel porphyrins. The literature provides an almost complete assignment of the observed Raman bands for the investigated nickel porphyrins,[25−28] which are listed in Table 1. For a particular mode, the frequencies are very similar, but the intensities vary considerably. Besides the oop modes, some in-plane A_{1g} modes such as ν_7, ν_8, ν_9 have been indicated in the spectra. All these bands are polarized, indicating that the distortions mostly responsible for the observed Raman activity have the same symmetry as the respective normal mode. Raman bands assign-

TABLE 1: Assignment for the Raman Bands of Nickel Porphyrins

Prominent Raman Bands of Porphyrins

	NiOEP	NiTPP	NiOETPP	NiT(^{i}Pr)P	NiT(^{t}Bu)P
γ_2	340				
γ_6	359				
γ_{10}		330		402	418
γ_{12}		551		544	546
γ_{11}					793
γ_{13}		904		895	898
γ_{15}			726		
γ_{16}			476		
γ_{17}			313		
ν_2	1600	1571	1560	1550	1530
ν_3	1517		1505	1453	1430
ν_4	1383	1371	1361	1369	1354
ν_6					943
ν_7			628/906	578	590
ν_8	361/343	391/404	362/379	354	359
ν_9			271		

Identified Franck−Condon Active Oop Modes in Raman Spectra of Nonplanar Porphyrins

	oop modes	
	ruffling modes (B_{1u}: γ_{10}−γ_{14})	saddling modes (B_{2u}: γ_{15}−γ_{18})
NiTPP	330 (γ_{10}), 551 (γ_{12}), 904 (γ_{13})	
NiOETPP		726 (γ_{15}), 476 (γ_{16}), 313 (γ_{17})
NiT(^{i}Pr)P	402 (γ_{10}), 544 (γ_{12}), 895 (γ_{13})	
NiT(^{t}Bu)P	418 (γ_{10}), 793 (γ_{11}), 546 (γ_{12}), 898 (γ_{13})	

able to B_{1u} modes appear in the spectra of NiTPP, NiT(^{i}Pr)P, and NiT(^{t}Bu)P, indicating that the corresponding macrocycle is subject to B_{1u} deformations. In contrast, the spectrum of NiOETPP displays bands attributable solely to modes of B_{2u} symmetry, suggesting a deformation of this symmetry type. In the following, we focus on these four porphyrins to investigate the relationship between nonplanar deformations and the Raman activity of oop modes.

Correlation between Oop Macrocycle Deformation and Oop Raman Modes. As discussed in the Theoretical Background section, nonplanar deformations change the ideal D_{4h} symmetry of the porphyrin macrocycle, so that out-of-plane modes can become Raman active. As a consequence, the oop modes become active with Soret excitation, mainly via Franck−Condon coupling. The intensities of Raman bands of oop modes observed with Soret excitation reflect the ground and excited state deformations along normal coordinates of the same D_{4h} symmetry representation. NiT(^{i}Pr)P and NiT(^{t}Bu)P, for example, are predominantly ruffled (as shown by the SNCD data in Table 2), and as a consequence it seems logical that the B_{1u}-type bands γ_{10}, γ_{12} appear relatively intense in the low frequency Raman spectra. Consistent with the idea that static deformations strongly influence the Raman spectra, for NiOETPP, where saddling is the dominant oop deformation (Table 2), the B_{2u} modes γ_{15}, γ_{16}, and γ_{17} bands are intense in the Raman spectrum.

However, it is not a priori clear that first-order SNCDs, which occur along the normal coordinates of lowest frequency, are responsible for the observed Raman intensities. The work of Haddad et al.[17] suggests that small, higher order deformations are at least as effectively coupled to the electronic B-states as low order (low wavenumber) deformations. One can imagine a similar scenario for the Raman activities of oop modes. Our recent work on horseradish peroxidase C suggests that the deformations of the minimal basis set are indeed predominantly

TABLE 2: In-Plane (A_{1g}) and Out-of-Plane Deformations (Å) Obtained from a NSD Analysis of the Investigated Nickel Porphyrins

basis	A_{1g}	B_{2u}	B_{1u}	A_{2u}	A_{1u}	E_{gx}	E_{gy}
NiTPP, X-ray Structure (ZZZUUC01)							
1st order	−0.322	−0.254	−1.266	0	0	0	0
2nd order	0.046	0.080	−0.005	0.001	0	0	0
3rd order	−0.003	0.004	−0.033	0.	0	0	0
NiT(^{i}Pr)P, Molecular Mechanics Calculations							
1st order	−0.660	0.029	2.203	0	0	0	0
2nd order	0.250	−0.012	0.186	0	0	0	0
3rd order	0.441	0.042	0.082	0.0	0	0	0
NiT(^{i}Pr)P, X-ray Structure (HETDAL)							
1st order	−0.564	−0.458	2.029	−0.026	0.025	−0.081	0.096
2nd order	0.171	−0.006	0.042	−0.004	−0.007	0.034	−0.017
3rd order	0.02	0.006	0.031	−0.005	0	−0.008	−0.013
NiT(^{t}Bu)P, Molecular Mechanics Calculations							
1st order	−0.973	0.005	2.279	0	0	0	0
2nd order	0.473	−0.001	0.323	0	0	0	0
3rd order	0.101	0.0	0.1	0	0	0	0
NiOETPP, X-ray Structure (SULCUX)							
1st order	−1.022	−3.805	0.091	−0.054	0.009	−0.060	−0.019
2nd order	−0.317	0.205	−0.011	0.026	0	0.031	0.018
3rd order	−0.342	0.043	0.002	0.0	0	−0.001	0.006

TABLE 3: Relative Intensities (I) and Depolarization Ratios (ρ) of the Raman Bands Assignable to the Prominent A_{1g} Ip Modes and the Oop Modes of Porphyrins in CH_2Cl_2[a]

NiT(^{i}Pr)P

	γ_{10}	γ_{12}	γ_{13}	ν_8	ν_4	ν_3	ν_2
$\tilde{\nu}$ [cm^{-1}]	403	558	896	354	1367	1453	1550
$I_{\|\|}$	0.64	0.27	0.27	1.32	0.49	0.22	1.3
ρ	0.18	0.16	0.15	0.18	0.25	0.20	0.16

NiT(^{t}Bu)P

	γ_{10}	γ_{11}	γ_{12}	γ_{13}	ν_8	ν_4	ν_3	ν_2
$\tilde{\nu}$[cm^{-1}]	418	792	546	899	360	1352	1430	1530
$I_{\|\|}$	0.33	0.12	0.56	0.26	0.72	0.96	0.33	0.82
ρ	0.22	0.27	0.19	0.26	0.17	0.22	0.29	0.14

NiOETPP

	γ_{15}	γ_{16}	γ_{17}	ν_8	ν_4	ν_3	ν_2
$\tilde{\nu}$ [cm^{-1}]	726	475	314	382	1360	1505	1560
$I_{\|\|}$	0.11	1.6	2.7	0.73	1.36	2.1	3.4
ρ	0.38	0.24	0.18	0.14	0.18	0.28	0.16

NiTPP

	γ_{10}	γ_{12}	γ_{13}	ν_8	ν_4	ν_2
$\tilde{\nu}$ [cm^{-1}]	333	555	889	406	1372	1572
$I_{\|\|}$	0.10	0.14	0.11	0.41	0.14	0.15
ρ	0.12	0.34	0.22	0.17	0.18	0.15

[a] Intensities are normalized to the internal standard of CH_2Cl_2 at 286 cm^{-1} in the Raman spectra.

responsible for the Raman activity of the oop modes.[13] In what follows, we determine whether or not this is also the case for the nickel porphyrins investigated.

Analysis of Intensities and Depolarization Ratios of Oop Bands. Thus far, we have interpreted the Raman activity of oop modes solely in terms of Franck−Condon coupling induced by the same symmetry deformation. If this was the exclusive contribution to the Raman tensor, the respective DPR values would be 0.125. An analysis of the polarized Raman spectra in Figure 2 reveals that this is not the case (cf. the DPR values in Table 3). While the DPRs of the Raman bands of typical A_{1g} ip modes are only slightly larger than the expected D_{4h} values, the corresponding values of most of the oop modes deviate substantially from 0.125. For instance, the B_{1u} mode γ_{13} in

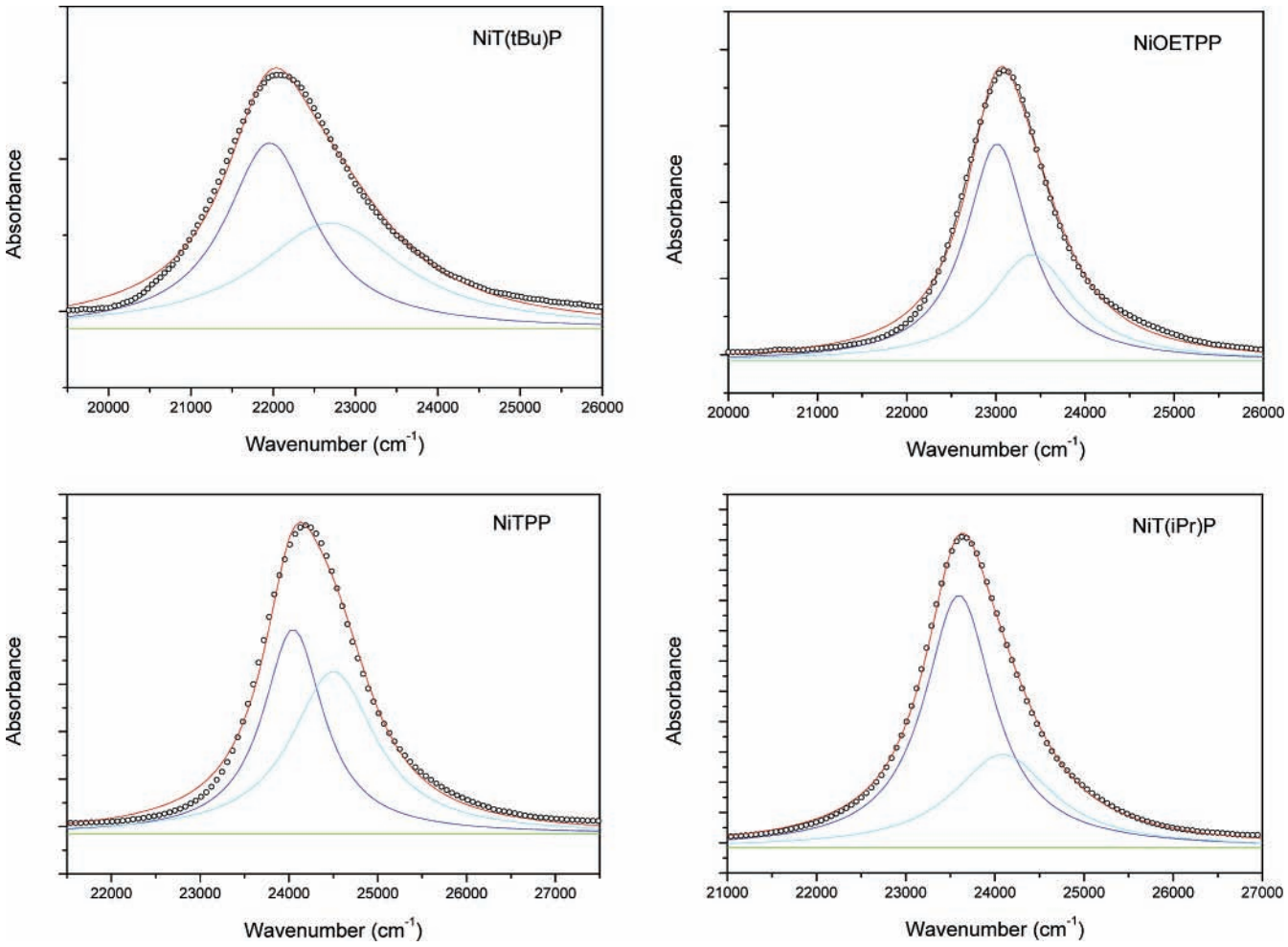

Figure 3. Absorption spectra of nickel porphyrins in CH_2Cl_2. The solid, colored lines result from a heuristic decomposition analysis of the B-band profiles into the respective B_0 (blue lines) and B_v (cyan lines) bands.

NiT(^{t}Bu)P exhibits a DPR of 0.26; in NiTPP, the B_{1u} mode γ_{12} exhibits a DPR value of 0.34; and in NiOETPP, the DPR of the B_{2u} mode γ_{15} exhibits an even larger value of 0.38.

To rationalize the large DPR values of the oop modes, we must consider deformations of different symmetry types. The second term in eq 1 can contribute terms which do not transform like A_{1g}. Let us, for example, consider a B_{2u}-mode. If additional deformations of A_{2u} and A_{1u} symmetry exist, the vibronic coupling operator will transform like $B_{2u} \otimes A_{2u} = B_{1g}$ and $B_{2u} \otimes A_{1u} = B_{2g}$, respectively. When it is admixed to total symmetric contributions $B_{2u} \otimes B_{2u} = A_{1g}$, the depolarization ratio increases. This seems to be the case for NiOETPP. The X-ray structure of NiOETPP reveals some A_{2u} deformation (−0.054 Å), which amounts to only about 1.5% of the dominant saddling deformation (3.8 Å). We therefore conclude that the deformation along this coordinate is either larger in solution or that the matrix elements $\langle B|\partial^2\hat{H}_{el}/\partial q_r^{B_{1u}}\partial q_j^{A_{2u}}|B\rangle$ are particularly large. If the former notion was correct, we would expect similar depolarization ratios for all three bands arising from B_{2u} modes. The values in Table 3 suggest that this is not the case. Hence, it follows that vibronic coupling strength rather than the magnitude of the A_{2u} (doming) deformation causes the increase of the depolarization ratios. This is an important finding in that it reveals that the depolarization ratio is a very sensitive tool for probing even subtle oop deformations.

The same concept can be invoked to explain the high DPR values of the remaining porphyrins. For NiTPP, the X-ray structure reveals an admixture of saddling (B_{2u}) with the dominant B_{1u} deformation, which leads to a $B_{1u} \otimes B_{2u} = A_{2g}$ admixture to the Raman tensor. Scattering induced by vibronic coupling of this symmetry is generally difficult to detect with B-band excitation,[18] which suggest that the corresponding matrix element $\langle B|\partial^2\hat{H}_{el}/\partial q_r^{B_{1u}}\partial q_j^{B_{2u}}|B\rangle$ is large enough to compensate for this deficiency. Moreover, the absolute and relative strength of the first-order B_{2u} deformation is significantly larger (−0.25 Å, 20% of the corresponding ruffling deformation, Table 2) than is the case for the A_{2u} deformation of NiOETPP. For NiT(^{i}Pr)P and NiT(^{t}Bu)P, additional B_{2u} deformations admix B_{1g} terms to the Raman tensors which results in larger DPR values.

At Soret excitation, the Franck−Condon induced Raman activity of E_g modes results exclusively from E_g-type deformations. Since the (first order) vibronic coupling operator transforms like $E_g \otimes E_g = A_{1g} + B_{1g} + B_{2g} + A_{2g}$, the depolarization ratio can vary between 0.125 and infinity even in the absence of deformations of different symmetry. Thus, specific information about heme deformations cannot be inferred from the respective depolarization ratios.

Determination of Vibronic Coupling Parameters. In order to use eq 4 in ref 13 to simulate the Raman intensities, we have to determine transition energies, dipole moment, damping and vibronic coupling constants $c_{BB}^{\Gamma_r}$ of the electronic transition into the B-state. In a first step, the respective B-band profiles of the investigated porphyrins were heuristically decomposed into two Lorentzian bands representing B_0 and B_v, as illustrated in Figure 3, to obtain the band positions E_{B0} and E_{Bv}, the bandwidths

TABLE 4: Spectral Parameters and Relative Dipole Strengths Obtained from a Heuristic Decomposition of the Soret Band

	E_{B0} [cm^{-1}]	Γ_{B0} [cm^{-1}]	E_{Bv} [cm^{-1}]	Γ_{Bv} [cm^{-1}]	R_{B0}	R_{B0}/R_{Bv}
NiTPP	24046	823	24500	1149	1	1
NiOETPP	23014	855	23396	1163	1.22	1.2
NiT(^{i}Pr)P	23596	939	24086	1342	1.13	1.4
NiT(^{t}Bu)P	21939	1283	22718	1803	0.97	1.2

TABLE 5: Relative Raman Intensities and Vibronic Coupling Constants c_{BB} for the ν_4 Mode in the Spectra of Nickel Porphyrins

ν_4	NiOETPP	NiT(^{i}Pr)P	NiT(^{t}Bu)P	NiTPP
relative intensity	1	0.1	0.53	0.05
c_{BB} [cm^{-1}]	120	90	250	114

Γ_{B0} and Γ_{Bv}, and the relative electronic transition dipole moments R_{B0} and R_{Bv} of the B-band and its vibronic sideband B_v, respectively. In principle, inhomogeneous broadening and vibronic coupling to a bath of low frequency modes brings about a convolution of the respective Lorentzians with a Gaussian profile.[29−31] The corresponding convolution integral for the Raman tensor has been reported earlier.[31] Since the current study is not aimed at an exact modeling of experimentally obtained resonance excitation profiles, we confined ourselves to using a Lorentzian approximation for the Raman analysis. The parameter values obtained from this band analysis are listed in Table 4.

Apparently, the Γ_{B0} values of the different porphyrins are similar. The different peak positions of the B-bands reflect a different degree of nonplanarity (ruffling), which has been shown to cause a red-shift of their first moments.[17] There are also significant differences between the R_{B0}/R_{Bv} ratio of the transition dipole moments of B_0 and B_v[32] between the nonplanar porphyrins and relatively planar porphyrins. For porphyrins with small oop deformations, such as NiP and NiOEP, the dipole moment of B_0 is nearly twice that of B_v. However, for porphyrins with larger oop deformations, such as NiOETPP and NiT(^{t}Bu)P, the transition dipole moment ratio approaches 1. The SNCD values in Table 2 indicate two reasons for this enhancement of the overall vibronic coupling strength in nonplanar porphyrins. First, the respective oop modes contribute to the B-band via Franck−Condon, and in the case of B_{1g}-type contributions, via Jahn−Teller coupling.[33] Second, the SNCD values reveal substantial A_{1g}-deformations of the nonplanar porphyrins, which adds additional Franck−Condon coupling to all A_{1g}-type modes via the second term in eq 1, namely, $\langle B|\partial^2\hat{H}_{el}/\partial q_r^{A_{1g}}\partial q_j^{A_{1g}}|B\rangle q_r^{A_{1g}}\delta\bar{q}_r^{A_{1g}}$. Additionally, for NiTPP and NiOETPP, phenyl modes become Raman active due to vibrational mixing with macrocycle vibrations and therefore contribute to the B_v-band as well.[31] This explains the particularly small R_{B0}/R_{Bv} value obtained for NiTPP. We therefore conclude that the $R(B_0)/R(B_v)$ ratio is an easily measured and useful indicator of nonplanar deformation in some porphyrin systems.

In a second step, we quantitatively analyzed and compared the Raman intensities of the investigated porphyrins. The procedure was aimed at a self-consistent description of Raman intensities and optical absorption. Our analysis was based on the following assumptions. First, we neglected the contributions from interstate Herzberg−Teller coupling to the Raman tensor, since the excitation wavenumber is close enough to the B-band position to guarantee the predominance of the scattering amplitudes arising from intrastate BB-coupling.[18] Second, since we excited at the low wavenumber side of the B-band, we could neglect the contributions from multimode mixing.[9] Therefore,

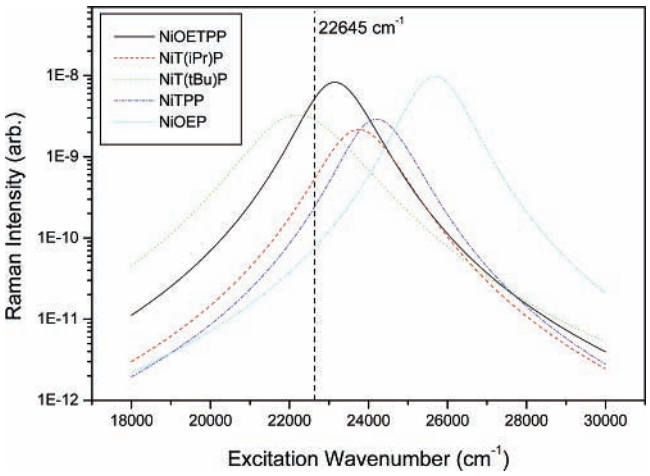

Figure 4. Simulations of the B-band resonance Raman excitation profiles (REP) of the ν_4 band in nonplanar porphyrins, which reproduce the Raman intensity ratios at 442 nm excitation observed experimentally. The simulations are based on single mode model for Raman scattering. The vibronic coupling constants used in the simulation are listed in Table 5. The respective simulation for NiOETPP has already been reported in ref 31.

the Raman intensities are mainly due to Franck−Condon coupling to the transition into the excited B state, i.e., reflected by the parameter $c_{BB}^{A_{1g}}$. We estimated $c_{BB}^{A_{1g}}$ of oop modes for all the porphyrins from their Raman spectra in the following way. First, we calibrated the Raman intensities by comparing them to the internal standard solvent band at 286 cm^{-1}, so we obtained the relative intensities

$$I'_{por} = I_{por}/I_{286} \tag{3}$$

for each porphyrin. Next, we used the ν_4 band of NiOETPP as a reference and compared the intensities of Raman bands of interest in other porphyrins to the NiOETPP reference. In the comparison, we took into account different concentrations and corrected for multiabsorption in the backscattering geometry. The former must be considered because of large differences in the porphyrin concentrations employed in our experiments, whereas the latter was found to be negligibly small (a factor around 1). Thus, the intensities were calibrated as

$$\frac{I'_x}{I'_{NiOETPP}} \approx \frac{n_x}{n_{NiOETPP}} \frac{\sigma_x}{\sigma_{NiOETPP}} \tag{4}$$

where n represents the respective porphyrin concentrations and x symbolizes the porphyrin being investigated. σ_x and $\sigma_{NiOETPP}$ denote the Raman cross sections of "x" and NiOETPP at 442 nm excitation, respectively. We utilized ν_4 of NiOETPP in the calibration because its coupling parameter has been determined from resonance excitation profiles (ca. −100 cm^{-1}).[31] Therefore, we could estimate the $|c_{BB}^{A_{1g}}|$ for ν_4 bands for the other porphyrins, and then obtain all the B-band vibronic coupling constants $|c_{BB}^{A_{1g}}|$ for the oop modes of interest for these porphyrins.

The coupling constants of the ν_4 band of the three *meso*-substituted porphyrins were obtained by using eq 4 in ref 13 to calculate the Raman intensity at 442 nm excitation. The respective Franck−Condon coupling parameters were varied to reproduce the experimental Raman intensity ratios of 1:0.1:0.53:0.05 for NiOETPP, NiT(^{i}Pr)P, NiT(^{t}Bu)P, and NiTPP, respectively. The resonance Raman excitation profiles are shown in Figure 4. Thus, we obtained coupling constants of 120, 90, 250,

TABLE 6: Vibronic Coupling Constants c_{BB} and Huang−Rice *S* Values of Oop Modes and A_{1g} Ip Mode as Derived from a Self-Consistent Analysis of the Raman Intensities and the Absorption Spectra of the Nickel Porphyrins

	NiT(^{i}PrP)			NiT(^{t}Bu)P				NiTPP			NiOETPP		
	γ_{10}	γ_{12}	γ_{13}	γ_{10}	γ_{11}	γ_{12}	γ_{13}	γ_{10}	γ_{12}	γ_{13}	γ_{15}	γ_{16}	γ_{17}
Ω_r [cm^{-1}]	403	558	896	418	792	546	899	333	555	889	726	475	314
c_{BB} [cm^{-1}]	102	67	67	144	87	188	128	96	114	100	34	130	170
S	0.064	0.014	0.006	0.12	0.012	0.12	0.02	0.083	0.042	0.013	0.002	0.075	0.3

	NiT(^{i}PrP)					NiT(^{t}Bu)P					NiTPP			NiOETPP				
	ν_8	ν_7	ν_4	ν_3	ν_2	ν_8	ν_7	ν_4	ν_3	ν_2	ν_8	ν_4	ν_2	ν_8	ν_7/ν'_7	ν_4	ν_3	ν_2
Ω_r [cm^{-1}]	354	578	1367	1453	1550	360	590	1352	1430	1530	408	1372	1572	382	628/906	1360	1505	1560
c_{BB} [cm^{-1}]	148	106	90	60	146	214	279	250	146	228	196	114	115	88	61/53	120	149	190
S	0.17	0.03	0.004	0.002	0.009	0.35	0.22	0.03	0.01	0.022	0.23	0.007	0.005	0.053	0.01/0.003	0.008	0.01	0.015

and 114 cm^{-1} for NiOETPP, NiT(^{i}Pr)P, NiT(^{t}Bu)P, and NiTPP, respectively.

We compared the Raman intensities of other bands with respect to the Raman intensity of ν_4 for each porphyrin, and thus obtained the coupling constants for other modes of interest, especially the oop modes and the prominent ip modes of A_{1g} symmetry. Table 6 lists the coupling parameters obtained using this procedure. It should be noted that the listed c_{BB} values are effective coupling parameters, which may encompass Franck−Condon ($c_{BB}^{A_{1g}}$) and Jahn−Teller ($c_{BB}^{B_{1g}}$) coupling. A decomposition into these symmetry related coupling strengths based on depolarization ratios is discussed below.

The validity of the coupling constants was checked by using them to calculate the absorption profiles of the B-band. To this end we used the equation[34]

$$L(\Omega_{abs}) \propto \sum_{\{m_j\}} \left\{ \prod_{m_j!}^{N} \frac{S_j^{m_j} e^{-S_j}}{m_j!} \frac{\Gamma/2}{(E_B + \sum_{j=1}^{N} m_j \Omega_j - \Omega_{abs})^2 + (\Gamma/2)^2} \right\} \quad (5)$$

where *S* is the Huang−Rice coefficient written as

$$S_j = \left(\frac{c_{BB}}{\Omega_j}\right)^2 \quad (6)$$

Ω_j is the wavenumber of the *j*th vibration contributing to the vibronic sideband B_v, and m_j is the vibrational quantum number of this vibration. The vibronic sideband is generally dominated by contributions from $m_j = 1$. It should be emphasized that eq 5 provides a very general description of all transitions into the vibronic manifold associated with the Franck−Condon coupling to a distinct electronic transition. As seen from eq 6, *S* can be derived from c_{BB}, and it can also be obtained by fitting the absorption profile using eq 5. The *S* values obtained from the Raman data are listed in Table 6. Interestingly, ν_8 exhibits a relatively large *S* value for all porphyrins, especially for NiT(^{t}Bu)P (for which the coupling of ν_7 also appears to be particularly strong). With respect to the oop modes, the contribution of B_v comes from different modes in different porphyrins, owing to their respective symmetry. For NiT(^{i}Pr)P, γ_{10} exhibits the strongest coupling; for NiT(^{t}Bu)P, both γ_{10} and γ_{12} are dominant; and for NiOETPP, γ_{16} and γ_{17} couple most effectively to the B-state transition.

We employed the coupling constants obtained from the Raman spectra in eq 5, to reproduce the experimental absorption profiles to a very satisfactory level, as shown in Figure 5. This clearly shows the reliability of the obtained coupling constants.

Estimation of Oop Deformations. The total ground state deformation δQ^{Γ_j} along coordinates of the *j*th out-of-plane mode can be obtained as the weighted sum of the respective displacements of each involved atom of the macrocycle:[13,31]

$$\delta\vec{Q}^{\Gamma_j} = \sqrt{\sum_i (T_j \Delta_{ij})^2 m_i} \approx T_j \sqrt{\sum_i (\Delta_{ij})^2 m_i} \quad (7)$$

where Δ_{ij} and m_i are the displacement and mass of the *i*th atom in the *j*th oop mode. The values of Δ_{ij} are obtained from the normal mode analysis of NiOEP.[26] T_j is a scaling factor reflecting the deformation induced by peripheral substituents.

For the first step of our analysis, we tentatively assumed that the observed Raman intensities of oop modes result solely from deformation along the normal coordinate of the respective Raman mode. A lower limit for $\delta\bar{Q}_{min}^{\Gamma_r}$ can be estimated by comparing the coupling parameters of the oop mode with the vibronic matrix element of the corresponding overtone:

$$\bar{c}_{BB} = \left\langle B \left| \frac{\partial^2 H}{\partial Q_r \, \partial Q_r} \right| B \right\rangle Q_r Q_r \quad (8)$$

Since no overtone intensity could be detected for all oop modes investigated, it follows that

$$\frac{c_{BB}}{\bar{c}_{BB}} = \frac{\delta\bar{Q}^{\Gamma_r}}{Q_r} \geq \sqrt{\frac{S_r}{N}} \quad (9)$$

where S_r/N is the observed signal-to-noise ratio of the Raman band of the *r*th Raman active oop mode. We determined S_r/N from the Raman spectra and obtained the $\delta\bar{Q}_{min}^{\Gamma_r}$ values listed in Table 7. Then we used eq 7 to scale $T_{r,min}\Delta_{ir}$ in order to reproduce $\delta\bar{Q}_{min}^{\Gamma_t} = \sqrt{\sum_i (T_r\Delta_{ir})^2} = T_r\sqrt{\sum_i (\Delta_{ir})^2}$ along the normal coordinate Q_r listed in Table 7. Finally, we used $\Delta_{min}^{\Gamma_r} = \sqrt{\sum_i (T_{r,min}\Delta_{ir})^2}$ to calculate the minimal total displacement.

A comparison with the respective NSD deformations listed in Table 2 revealed that all deformations along the normal coordinates of the higher frequency modes are too small to explain the coupling strengths of the investigated oop modes. Only for NiT(^{t}Bu)P is the amount of a higher order deformation of B_{1u}-symmetry ($2B_{1u}$) close to our estimation (0.19−0.45 Å). However, the structure of NiT(^{t}Bu)P resulted from molecular mechanics calculations, which are thought to overestimate the higher order B_{1u} deformations.[14] This effect is seen for the case of NiT(^{i}Pr)P (Table 2), where X-ray[35] and molecular mechanics structures are available. This consideration and the fact that the above estimation yields the lower limit for the respective deformations comparison lead us to conclude that the NSD deformations along the coordinates of the lowest frequency

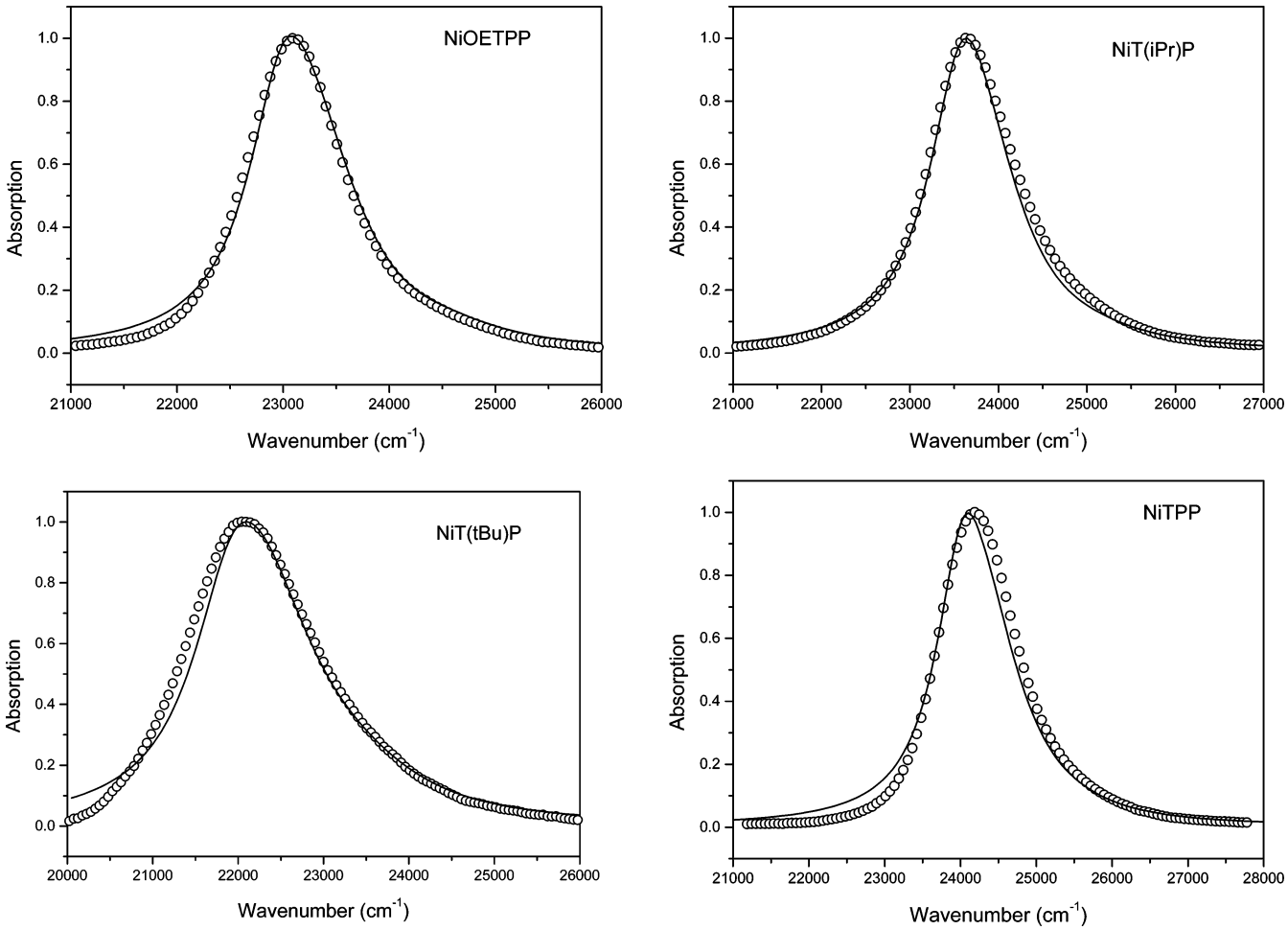

Figure 5. Simulation of the Soret absorption profiles of nonplanar nickel porphyrins based on the vibronic coupling parameters obtained from the band intensities in the respective Raman spectra taken with 442 nm excitation.

TABLE 7: Oop Deformations and Displacements of Excited State Derived from Vibronic Coupling Parameters of Ip and Oop Modes of the Nickel Porphyrins in Solution

	NiT(^{i}PrP)			NiT(^{t}Bu)P				NiTPP			NiOETPP		
	γ_{10}	γ_{12}	γ_{13}	γ_{10}	γ_{11}	γ_{12}	γ_{13}	γ_{10}	γ_{12}	γ_{13}	γ_{15}	γ_{16}	γ_{17}
Ω_r [cm^{-1}]	403	558	896	418	792	546	899	333	555	889	726	475	314
Q_r [(kg$^{1/2}$ Å) $\times$ 10^{-15}]	8.5	7.2	5.7	8.3	6.0	7.3	5.7	9.3	7.2	5.7	6.3	7.8	9.6
δQ_r [(kg$^{1/2}$ Å) $\times$ 10^{-15}]	30	16	12	60	26	64	36	22	20	14	12	58	92
ΔQ_r [(Å)]	0.21	0.11	0.08	0.43	0.19	0.45	0.26	0.14	0.14	0.10	0.08	0.41	0.65

modes (1Γ) are the predominant cause for the observed Raman activity of the oop modes.

We then estimated the matrix elements $\langle B|\partial^2\hat{H}_{el}/\partial Q_r^{\Gamma_r}\partial Q_{lw}^{\Gamma_{lw}}|B\rangle$ for the Raman activity induced by deformations along the normal coordinate $\delta\bar{q}_{lw}^{\Gamma_{lw}}$ of the lowest wavenumber vibration of a given symmetry Γ_{lw}. This is aimed at obtaining structural information about the excited B-state and at identifying oop modes the Raman intensity of which can be used to quantitatively determine oop deformations in other porphyrins. To be more accurate, we had to consider that the depolarization ratios of the oop modes (Table 3) are larger than the ideal value of 0.125. Therefore, we have to disentangle the contributions arising from $A_{1g}(\Gamma_{hw} = \Gamma_r)$ and B_{1g}/B_{2g} type coupling ($\Gamma_{hw} = B_{2u}$ for $\Gamma_r = A_{2u}$, $\Gamma_{hw} = A_{2u}$ for $\Gamma_r = B_{2u}$ and $\Gamma_r = B_{1u}$) to the Raman tensor. As shown recently,[13] this can be achieved by using the equation

$$|c_{BB}^{A_{1g}}| \approx \frac{|c_{BB}|}{1+r} \tag{10}$$

with

$$r = \left|\frac{c_{BB}^{B}}{c_{BB}^{A_{1g}}}\right| = \sqrt{\frac{8\rho - 1}{3 - 4\rho}} \tag{11}$$

The thus obtained $|c_{BB}^{A_{1g}}|$ and the related $|c_{BB}^{B}|$ (B: B_{1g} or B_{2g}) values are listed in Table 8. The former are up to a factor of 2 smaller than the respective $|c_{BB}|$ values.

Finally, we used the value of $|c_{BB}^{A_{1g}}|$ to estimate $\langle B|\partial^2\hat{H}_{el}/\partial Q_r^{\Gamma_r}\partial Q_{lw}^{\Gamma_{lw}}|B\rangle$ based on the assumption that deformations along the lowest wavenumber coordinates are predominantly responsible for the Raman activity of all oop modes.

The values listed in Table 8 led us to the following conclusions:

(1) The coupling strength of B_{1u}-modes is systematically larger than that of B_{2u} modes, indicating a much larger deformation of the excited B-state along the coordinates of the B_{1u}-modes. In structural terms, this means that the excited state

TABLE 8: Vibronic Coupling Matrix Elements Due to Deformations along the Coordinates of the Lowest Frequency Oop Modes of the Nickel Porphyrins

	NiT(^{i}PrP)			NiT(^{t}Bu)P				NiTPP			NiOETPP		
	γ_{10}	γ_{12}	γ_{13}	γ_{10}	γ_{11}	γ_{12}	γ_{13}	γ_{10}	γ_{12}	γ_{13}	γ_{15}	γ_{16}	γ_{17}
$\lvert c_{BB}^{A_{1g}}\rvert$ [cm^{-1}]	72	50	51	105	48	127	76	96	57	73	16	78	120
$\lvert c_{BB}^{B}\rvert$ [cm^{-1}]	32	17	16	38	39	61	52	−(∼0)	57	26	19	53	53
$D_{BB}^{A_{1g}(lf)} = \langle B\lvert\partial^2 H/\partial Q_r^{\Gamma_r}\partial Q_{lf}^{\Gamma_{lf}=\Gamma_r}\rvert B\rangle$ [10^{28} cm^{-1} kg^{-1} Å^{-2}]	3.0	2.4	3.2	3.3	2.1	4.5	3.4	5.8	4.4	7.2	0.5	1.9	2.3
$D_{BB}^{B(lf)} = \langle B\lvert\partial^2 H/\partial Q_r^{\Gamma_r}\partial Q_{lf}^{\Gamma_{lf}}\rvert B\rangle$ [10^{28} cm^{-1} kg^{-1} Å^{-2}]	1.3	0.9	1.0	1.2	1.7	2.1	2.4	−(∼0)	4.4	2.6	0.6	1.3	1.1

is more ruffled than the ground state. This is in good agreement with recent theoretical calculations by Jarecki and Spiro, who investigated the Raman intensities of out-of-plane modes of free base porphine.[36] They found that one has to assume a saddling (B_{2u}) displacement of 1.2 Å to obtain intensities for the B_{2u}-modes that are in the same order of magnitude as those obtained for B_{1u}-modes induced by a ruffling (B_{1u}) deformation of only 0.5 Å.

(2) The coupling strengths of γ_{10} and γ_{13} are practically identical for NiT(^{i}Pr)P and NiT(^{t}Bu)P, whereas they are substantially larger for NiTPP. This suggests that the measured coupling strength of these two modes can be used to at least estimate the ruffling deformation of Ni−porphyrins with alkyl substituents attached at the *meso* positions. Since these substituents are unlikely to affect the macrocycle electronically, they might serve as suitable model systems for the heme groups in proteins. However, the role of the oxidation and spin state of the central iron atom still has to be elucidated. Interestingly, however, the coupling of 2.1×10^{30}/kg cm Å^2 obtained for γ_{11} of NiT(^{t}Bu)P is close to the value of 1.8×10^{30}/kg cm Å^2 recently observed for the ferric state of HRP C.[13]

(3) The coupling strength of γ_{12} is substantially larger in NiT(^{t}Bu)P than in NiT(^{i}Pr). This somewhat surprising result can be explained by invoking the results of the normal mode calculations by Unger et al., who found that ν_7 and γ_{12} are vibrationally mixed due to the ruffling deformation.[27] The coupling strength of ν_7 is substantially larger for NiT(^{t}Bu)P than for NiT(^{i}Pr). A part of this is transferred to the out-of-plane mode via vibrational mixing, thus making it unsuitable for determining ruffling deformations in other porphyrins. The larger coupling constants of ν_7 in NiT(^{t}Bu)P and also of ν_8 in NiT-(^{t}Bu)P, NiT(^{i}Pr), and NiTPP suggest that these modes gain Raman intensity when nonplanar deformations occur. This is a physically reasonable model, since the NSD analysis (Table 2) suggests a substantial increase in the in-plane A_{1g}-type deformations in the nonplanar porphyrins, which will affect the Raman cross section of in-plane mode via the second term in eq 1. These in-plane deformations can be a direct consequence of nonplanar deformations, as shown earlier.[17,31] This effect results from the oop deformation requiring a corresponding ip deformation, because the bonds in the porphyrin ring are relatively inflexible.

Conclusions

As shown in this study, nonplanar deformations of different symmetry types in nonplanar nickel porphyrins can be effectively probed by Raman spectroscopy. The B-band Franck−Condon induced Raman intensities of these oop modes stem mainly from the deformations along the normal coordinates of the lowest-frequency modes in a given symmetry block. These nonplanar deformations are the first-order oop deformations in the framework of NSD analysis, and are thought to affect the biological function of some heme proteins. Specifically, we found that $\gamma_{10}-\gamma_{13}$ are sensitive indicators of first-order ruffling deformation in NiTPP, NiT(^{i}Pr)P, and NiT(^{t}Bu)P, whereas $\gamma_{15}-\gamma_{17}$ are indicators of first-order saddling deformation in NiOETPP. The vibronic coupling strengths of all relevant in-plane and out-of-plane modes observable at Soret excitation have been determined by self-consistently analyzing the Raman intensities and depolarization ratios as well as the respective absorption spectra. Thus, we determined the coupling strengths of the out-of-plane modes. The results indicate that some of these modes can be used as a quantitative probe to determine the ruffling deformation of porphyrins with alkyl substituents at their *meso* positions.

Acknowledgment. We would like to thank John Shelnutt for his very kind help concerning the performance of NSD analyses. The project is supported by a grant from the National Science Foundation (MCB-0318749) to R.S.-S. Sandia is a multiprogram laboratory operated by Sandia Corporation, a Lockheed-Martin company, for the United States Department of Energy under Contract DE-ACO4-94AL85000.

References and Notes

(1) *The Porphyrins*; Dolphin, D., Ed.; Academic: New York, 1978; Vols. I−VI.

(2) Song, Y.; Haddard, R. E.; Jia, S.-L.; Hok, S.; Olmstead, M. M.; Nurco, D. J.; Schore, N. E.; Zhang, J.; Ma, J.-G.; Smith, K. M.; Gazeau, S.; Pécaut, J.; Marchon, J.-C.; Medforth C. J.; Shelnutt, J. A. *J. Am. Chem. Soc.* **2004**, *127*, 1179.

(3) Barkigia, K. M.; Chantranupong, L.; Smith, K. M.; Fajer, J. *J. Am. Chem. Soc.* **1991**, *113*, 4077.

(4) Jentzen, W.; Ma, J.-G.; Shelnutt, J. A. *Biophys. J.* **1998**, *74*, 7653.

(5) Kadish, K. M., Smith, K. M., Guilard, R., Eds. *The Porphyrin Handbook*; Academic Press: San Diego, 2000; Vol. 10.

(6) Stichternath, A.; Schweitzer-Stenner, R.; Dreybrodt, W.; Mak, R. S. W.; Li, X.-Y.; Sparks, L. D.; Shelnutt, J. A.; Medforth, C. J.; Smith, K. M. *J. Phys. Chem.* **1993**, *97*, 3701.

(7) Jentzen, W.; Unger, E.; Karvounis, G.; Shelnutt, J. A.; Dreybrodt, W.; Schweitzer-Stenner, R. *J. Phys. Chem.* **1996**, *100*, 14184.

(8) Jentzen, W.; Unger, E.; Song, X.-Z.; Jia, S.-L.; Turowska-Tyrk, I.; Schweitzer-Stenner, R.; Dreybrodt, W.; Scheidt, W. R.; Shelnutt, J. A. *J. Phys. Chem. A* **1997**, *101*, 5789.

(9) Schweitzer-Stenner, R. *Q. Rev. Biophys.* **1989**, *22*, 381.

(10) Huang, Q.; Szigeti, V.; Fidy, J.; Schweitzer-Stenner, R. *J. Phys. Chem. B* **2003**, *107*, 2822.

(11) Huang, Q.; Al-Azzam, W.; Griebenow, K.; Schweitzer-Stenner, R. *Biophys. J.* **2003**, *84*, 3285.

(12) Schweitzer-Stenner, R.; Cupane, A.; Leone, M.; Lemke, C.; Schott, J.; Dreybrodt, W. *J. Phys. Chem. B* **2000**, *104*, 4754.

(13) Huang, Q.; Schweitzer-Stenner, R. *J. Raman Spectrosc.* **2005**, *36*, 363.

(14) Shelnutt, J. A.; Song, X.-Z.; Ma, J.-G.; Jia, S.-L.; Jentzen, W.; Medforth, C. J. *Chem. Soc. Rev.* **1998**, *27*, 31.

(15) Jentzen, W.; Song, X.-Z.; Shelnutt, J. A. *J. Phys. Chem. B* **1997**, *101*, 1684.

(16) Shelnutt, J. A.; Medforth, C. J.; Berber, M. D.; Barkigia, K. M.; Smith, K. M. *J. Am. Chem. Soc.* **1991**, *113*, 4077.

(17) Haddad, R. E.; Gazeau, S.; Pecaut, J.; Marchon, J.-C.; Medforth, C. J.; Shelnutt, J. A. *J. Am. Chem. Soc.* **2003**, *125*, 1253.

(18) Schweitzer-Stenner, R. *J. Porphyrins Phthalocyanines* **2001**, *5*, 198.

(19) Shelnutt, J. A. In *Porphyrin Handbook*; Kadish, K. M., Smith, K. M., Guilard, R., Eds.; Academic Press: San Diego, 2000; Vol. 7, p 167.

(20) Unger, E.; Bobinger, U.; Dreybrodt, W.; Schweitzer-Stenner, R. *J. Phys. Chem.* **1993**, *97*, 9956.

(21) Levantino, M.; Huang, Q.; Cupane, A.; Laberge, M.; Hagarman, A.; Schweitzer-Stenner, R. *J. Chem. Phys.* **2005**, *123*, 05408.

(22) Ma, J.-G.; Laberge, M.; Song, X.-Z.; Jentzen, W.; Jia, S.-L.; Vanderkooi, J. M.; Shelnutt, J. A. *Biochemistry* **1998**, *37*, 5118.

(23) Shelnutt J. A. *J. Porphyrins Phthalocyanines* **2000**, *4*, 386.

(24) A web-based version of the NSD program is available at http://jasheln.unm.edu/jasheln/content/nsd/NSDengine/nsd_index.htm.

(25) Rush, T. S.; Kozlowski, P.; Piffat, C. A.; Kumble, R.; Zgierski, M. Z.; Spiro, T. G. *J. Phys. Chem. B* **2000**, *104*, 2050.

(26) Li, X. Y.; Czernuszewicz, R. S.; Kincaid, J. R.; Spiro, T. G. *J. Am. Chem. Soc*. **1989**, *111*, 7012.

(27) Unger, E.; Beck, M.; Lipski, R. J.; Dreybrodt, W.; Medforth, C. J.; Smith, K. M.; Schweitzer-Stenner, R. *J. Phys. Chem. B* **1999**, *103*, 10022.

(28) Tsai, H.-H.; Simpson, M. C. *J. Phys. Chem. A* **2004**, *108*, 1224.

(29) Schomaker, K. T.; Delaney, J. K.; Champion, P. M. *J. Chem. Phys.* **1986**, *85*, 4240.

(30) Cupane, A.; Leone, L.; Cordone, H.; Gilch, W.; Dreybrodt, W.; Unger, E.; Schweitzer-Stenner, R. *J. Phys. Chem.* **1996**, *100*, 14192.

(31) Schweitzer-Stenner, R.; Stichternath, A.; Dreybrodt, W.; Jentzen, W.; Song, Z. P.; Shelnutt, J. A.; Faurskov Nielson, O.; Medforth, C. J.; Smith, K. M. *J. Chem. Phys*. **1997**, *107*, 1794.

(32) This analysis assumes an effective dipole moment for the entire vibronic sideband associated with the B-state transition.

(33) Shelnutt, J. A.; Cheung, L. D.; Chang, R. C. C.; Yu, N. T.; Felton, R. H. *J. Chem. Phys.* **1977**, *66*, 3387.

(34) Cupane, A.; Leone, M.; Vitrano, E. *Eur. Biophys. J.* **1993**, *21*, 385.

(35) Ema, T.; Senge, M. O.; Nelson, N. Y.; Ogoshi, H.; Smith, K. M. *Angew. Chem., Int. Ed. Engl.* **1994**, *33*, 1879.

(36) Jarecki, A. A.; Spiro, T. G. *J. Phys. Chem. B* **2005**, *109*, 421.